Hindawi Publishing Corporation
Journal of Nanomaterials
Volume 2016, Article ID 5464978, 6 pages
http://dx.doi.org/10.1155/2016/5464978

*Research Article*

# Synthesis, Characterization, and NIR Reflectance of Highly Dispersed $NiTiO_3$ and $NiTiO_3/TiO_2$ Composite Pigments

**Yuping Tong, Jing Fu, and Zheng Chen**

*School of Civil Engineering and Communication, North China University of Water Resources and Electric Power, Zhengzhou 450011, China*

Correspondence should be addressed to Yuping Tong; tongqzm@163.com

Received 6 January 2016; Revised 22 March 2016; Accepted 27 March 2016

Academic Editor: Jean M. Greneche



The highly dispersed nanostructured $NiTiO_3$ pigments and $NiTiO_3/TiO_2$ composite pigments can be synthesized at relative low temperature. The activation energy of crystal growth of $NiTiO_3$ during calcinations via salt-assistant combustion method is 9.35 kJ/mol. The UV-vis spectra results revealed that the absorbance decreased with the increasing of calcinations temperature due to small size effect of nanometer particles. The optical data of $NiTiO_3$ nanocrystals were analyzed at the near-absorption edge. SEM showed that the obtained $NiTiO_3$ nanocrystals and $NiTiO_3/TiO_2$ nanocomposite were composed of highly dispersed spherical-like and spherical particles with uniform size distribution, respectively. The chromatic properties and diffuse reflectance of samples were investigated. The obtained $NiTiO_3/TiO_2$ composite samples have higher NIR reflectance than $NiTiO_3$ pigments.

## 1. Introduction

The temperature inside buildings can be potentially raised due to intense solar radiation to exterior surfaces. Rising energy cost drives people to explore new technologies designed to improve energy efficiency across the globe [1]. Recently, more and more interest has attended roofing materials with high NIR reflectance [2, 3]. The high NIR pigments as "cool" coating can help in maintaining lower exterior surface temperature of building; as a result, the indoor thermal comfort levels in hot season are improved. In recent years, many inorganic pigments have been extensively used as cool materials for building roofs and facades [4]. $TiO_2$, a white pigment with a high solar reflectance of about 87%, is regarded as the best pigment for coating materials, but its application is restricted because it easily causes "white pollution" [5]. There is an interest to develop new environment-friendly and sustainable "colored" pigment without toxic elements such as Pb, Hg, Cd, Sb, As, and Cr [6]. To date, special attentions have been paid to perovskite-type $NiTiO_3$, a traditional yellow-colored pigment, as chemical and electrical materials [7, 8]. In the structure of $NiTiO_3$, both Ni and Ti atoms prefer octahedral coordination with alternating cation layers occupied by Ni and Ti atoms alone, which gives it good stability [9, 10]. In particular, incorporation of $NiTiO_3$ into $TiO_2$ can be expected to obtain better "colored" pigment with high NIR reflectance.

A study indicated that nanocrystalline pigments had better solar reflectance properties compared with macrocrystalline pigments. It is well known that structure and properties of materials may be tailored by processing control. Recent efforts have focused on tailoring nanopigments by energy-saving method. Traditionally, in commercial processes, nanocrystalline $NiTiO_3$ can be prepared by solid state reaction, coprecipitation, high-energy ball milling process, sol-gel, sol-gel assisted electrospinning, and pyrolysis of polymeric precursor [7, 9, 11, 12]. Although these routes can produce nanosized $NiTiO_3$ particles, the dispersibility of nanoscale particles that has been reported is not so ideal. The salt-assistant self-propagation combustion method has been developed by our group for preparation of pyrochlore-type and spinel-type nanoparticles [13, 14]. In this paper, we presented the fabrication and properties of highly dispersed $NiTiO_3$ and $NiTiO_3/TiO_2$ nanoyellow pigments.

## 2. Experimental

*2.1. Preparation of Materials.* All reagents were of analytical grade and were used without further purification. In this work, $NiTiO_3$ was synthesized by a salt-assisted self-propagating combustion method (SSCM). Tetra-n-butyl titanate ($Ti(C_4H_9O)_4$) and nickel nitrate ($Ni(NO_3)_2{\cdot}6H_2O$) were used as the precursors of Ti and Ni, respectively. Critic acid was used as fuel. KCl was used as inert salt. Critic acid can not only act as fuel, but also act as a complexing agent with a variety of metal ions. According to the formula $NiTiO_3$, stoichiometric amount of $(Ni(NO_3)_2{\cdot}6H_2O)$, $Ti(C_4H_9O)_4$, and KCl were added to critic acid solution in turn. After a series of steps of magnetic force stirring, evaporating, and self-propagating combustion, the loose combustion product was obtained. The fabrication procedure was similar to the literature [13]. The combustion product was ground into powders and then submitted to calcine at 700°C~900°C for 4 h.

$NiTiO_3/TiO_2$ nanocomposite was prepared by a sol-gel procedure. A solution of $Ti(C_4H_9O)_4$ (as $TiO_2$ is 0.5 g) in 15 mL ethanol was dropped into a 100 mL $NiTiO_3$ (2 g, above obtained samples calcined at 700°C) water solution under stirring. The mixture was kept stirring for 5 h, followed by standing at room temperature for 24 h to get opaque gel. The obtained gels were kept at 80°C for 4 h and then dried at 90°C for 2 h. Finally, the obtained samples were calcined at 400°C for 3 h.

*2.2. Instrumentation.* The crystalline phase structure was determined by Bruker D8 Advance X-ray diffractometer (XRD) using Cu K$\alpha$ radiation. UV-vis absorption spectrum was carried out by UV-1700 spectrometer. Scanning electron microscopy (SEM) image was recorded on a JSM-7500F scanning electron microscope; EDS was taken on INCAPentaFET-x3 energy dispersive X-ray detector. The CIE 1976 $L^*a^*b^*$ colorimetric method was used, as recommended by the Commission Internationale de l'Eclairage (CIE). In this method, $L^*$ is the lightness axis [black (0) to white (100)], $a^*$ is the green (−value) to red (+value) axis, and $b^*$ is the blue (−value) to yellow (+value) axis. The parameter $C^*$ (chroma) represents saturation of the color. For each colorimetric parameter of a sample, measurements were made in triplicate and an average value was chosen as the result. Typically, for a given sample, the standard deviation of the measured CIE $L^*a^*b^*$ values is less than 0.10, and the relative standard deviation is not higher than 1%, indicating that the measurement error can be ignored. UV-vis-NIR reflectance of the obtained pigments was carried out by UV-vis-NIR spectrophotometer (PerkinElmer Lambda 950), using polytetrafluoroethylene (PTFE) as a white standard.

## 3. Results and Discussions

*3.1. XRD Analysis.* Figure 1 shows the XRD patterns of $NiTiO_3$ combustion product, after being ground and calcined at different temperatures for 4 h. All diffraction peaks are in good agreement with the reflection of ilmenite $NiTiO_3$ phase [11]. The peaks are indexed, corresponding to the lattice planes (012), (104), (110), (113), (024), (116), (124), and (300)

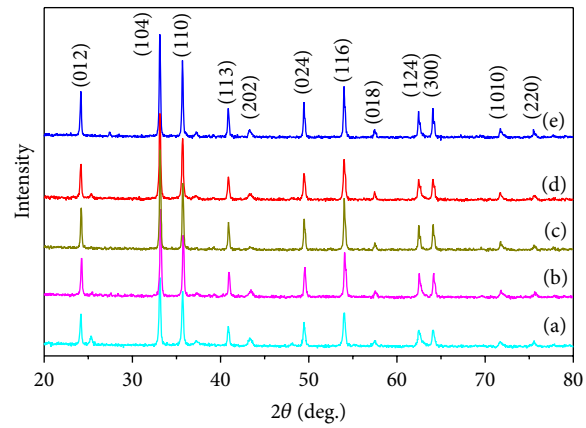


Figure 1: XRD patterns of $NiTiO_3$ combustion product calcined at (a) 700°C, (b) 750°C, (c) 800°C, (d) 850°C, and (e) 900°C for 4 h, respectively.

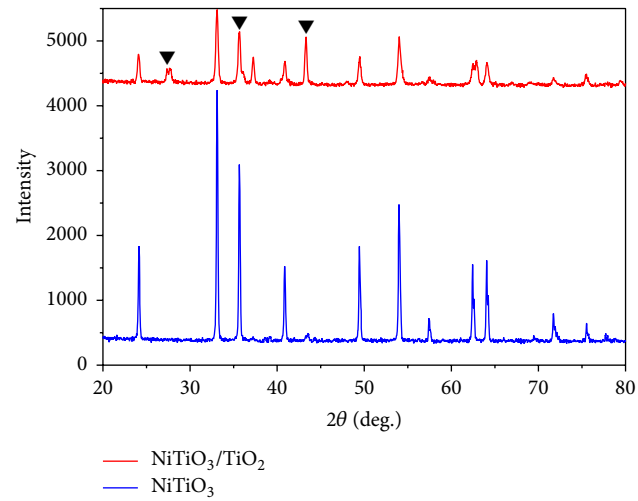


Figure 2: XRD patterns of samples: (a) $NiTiO_3$, (b) $NiTiO_3/TiO_2$; "▼" denotes the diffraction peaks of $TiO_2$.

of cubic system. It is noted that $NiTiO_3$ nanocrystals can be synthesized at 700°C. The lattice constant of samples is obtained by jade 6 program, the average crystal size is determined from the XRD patterns according to the Scherrer equation, and corresponding data are listed in Table 1. It is clear that, with the increasing of calcining temperature, both of the lattice constant and crystal size become larger to some extent. The activation energy $E$ for crystal growth is equal to 9.35 kJ/mol by calculation according to the literature [13].

XRD patterns of $NiTiO_3/TiO_2$ nanocomposite are shown in Figure 2. It has been illustrated that there exist the characteristic peaks of $TiO_2$ in the $NiTiO_3/TiO_2$ composite as anatase phase (JCPDS 73-1764) in comparison with XRD pattern of pure $NiTiO_3$. No other polymorph of $TiO_2$ is observed. Moreover, the intensity of $NiTiO_3$ peaks is significantly lower. It is indicated that to some extent $NiTiO_3$ are coated by $TiO_2$ particles. The results can be further confirmed by SEM and EDS.

Table 1: The lattice constant and crystal size of $NiTiO_3$ nanocrystals.

| | 700°C | 750°C | 800°C | 850°C | 900°C |
|---|---|---|---|---|---|
| $2\theta$ of crystal plane (104) | 33.112 | 33.113 | 33.109 | 33.109 | 33.111 |
| Lattice constant | | | | | |
| $a$ | 5.02912 | 5.02315 | 5.02985 | 5.02993 | 5.02982 |
| $c$ | 13.79037 | 13.77461 | 13.79002 | 13.79118 | 13.78966 |
| Crystal size | 46.9 | 49.3 | 58.1 | 63.0 | 65.3 |

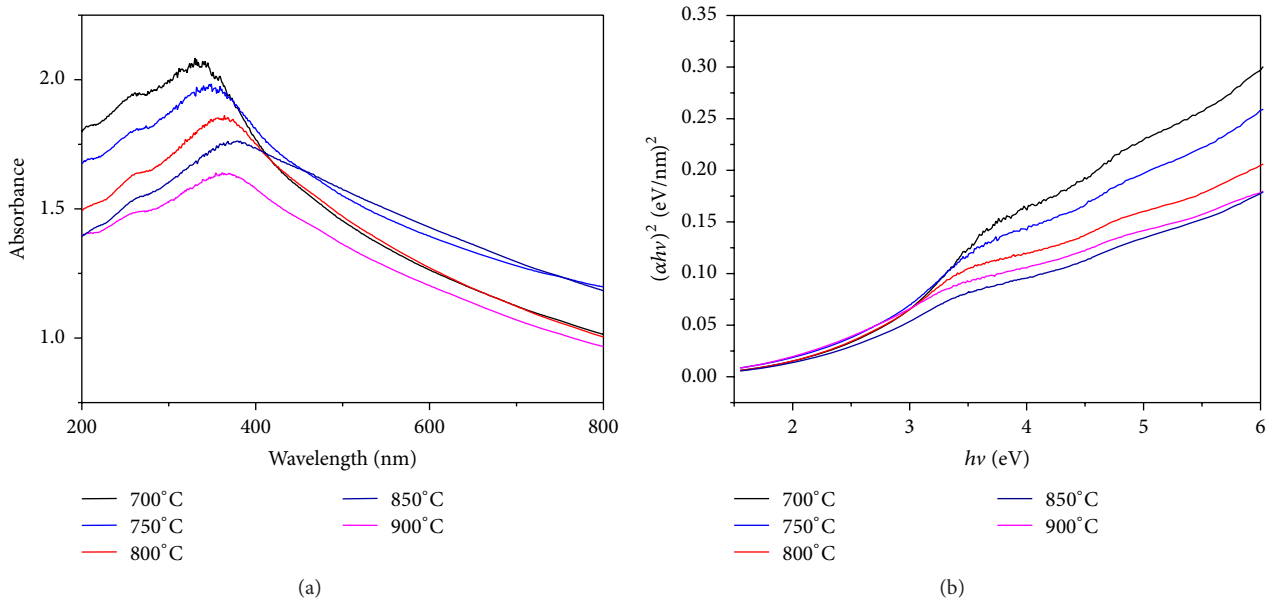


Figure 3: (a) UV-vis absorption spectra of $NiTiO_3$ precursor calcined at different temperatures; (b) $(\alpha h\nu)^2$ versus $h\nu$, showing the fit to linear portion corresponding to the direct band gap transition.

*3.2. UV-Vis Spectra Characteristic.* Figure 3 shows the UV-vis absorption spectra of $NiTiO_3$ precursor calcined at different temperatures (700°C, 750°C, 800°C, 850°C, and 900°C) in ethanol suspension prepared using 20 W/cm$^2$ sonic intensity for 5 mins. It can be seen that, with the increasing of calcinations temperature, the absorbance decreased, which can be attributed to small size effect of nanometer particles.

The optical data were analyzed at the near-absorption edge. According to the literature [12], the relation between the band gap of semiconductors for direct transition materials and absorption coefficient satisfied the following equation:

$$\alpha h\nu = K\left(h\nu - E_g\right)^{1/2}, \quad (1)$$

where $h\nu$ is Photon Energy, $\alpha$ is absorption coefficient, $K$ is constant in relation with the materials, and $E_g$ is the band gap of the semiconductors. Figure 4(b) shows the plot of $(\alpha h\nu)^2$ versus $h\nu$. The energy intercept gives $E_g$ for a direct transition when the linear region is extrapolated to zero ordinate. The band gap of $NiTiO_3$ precursor calcined at different temperatures (700°C, 750°C, 800°C, 850°C, and 900°C) is calculated to be 2.63 eV, 2.34 eV, 2.17 eV, 2.03 eV, and 2.09 eV, respectively. Generally, due to the quantization size effects, the band gap value decreased with the increasing of crystal size (Table 1). The value is smaller than that reported in [10], 2.92~3.16. As we all know, high-efficiency visible-light-driven semiconductor photocatalysis should have sufficiently narrow band gap with the value of 1.23 eV $< E_g <$ 3.0 eV [15]. On one hand, the band gap with $E_g < 3.0$ eV is to harvest visible light; on the other hand, large enough band gap with $E_g > 1.23$ eV is to provide energetic electrons. So the obtained samples can be considered as interesting candidates for use in photocatalysis.

*3.3. SEM and EDS Analysis.* The sample for SEM and EDS is made by the following steps. First, the sample was dispersed in ethanol with oscillating for 20 min in the ultrasonicator at constant temperature. Then the sample was dropped slowly on the silicon chip.

Figure 4(a) gives the SEM images of the $NiTiO_3$ pigments obtained at 700°C. It is clear that the sample is composed of highly dispersed and spherical-like particles and the size distribution is uniform. However, the size of 50~80 nm is larger than the value (46.9 nm) obtained from XRD patterns by the Scherrer formula. This is due to the fact that the crystal size obtained by the XRD is the grain size and that obtained by the SEM is particles' size.

The morphologies of $NiTiO_3/TiO_2$ nanocomposites are shown in Figure 4(b). It can be seen that the uniform and highly dispersed $NiTiO_3/TiO_2$ composite particles with

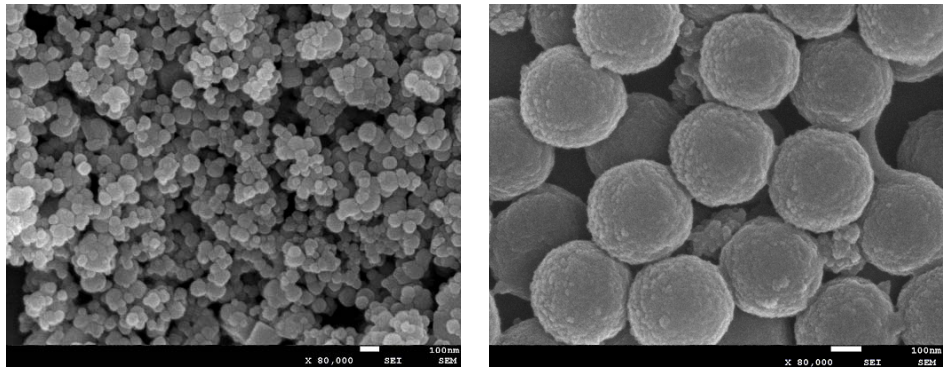

(a) (b)

Figure 4: SEM images of $NiTiO_3$ precursor calcined at 700°C; (b) $NiTiO_3/TiO_2$ composites.

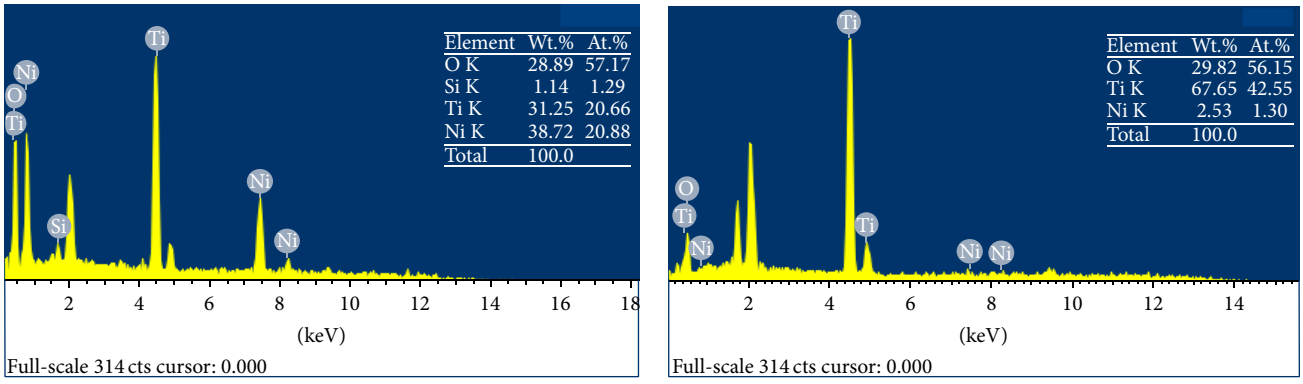


(a) (b)

Figure 5: EDS analysis of $NiTiO_3$ nanocrystals (a) and $NiTiO_3/TiO_2$ composites (b); insets indicate the amount of elements.

spherical shape are ca. 300 nm in diameter. Furthermore, we can see that the surface of sphere is not smooth and uniform but consists of many particles. The morphologies of $NiTiO_3/TiO_2$ nanocomposites reveal that $NiTiO_3$ nanoparticles are coated by $TiO_2$ particles.

EDS is used to further confirm the composition of the obtained samples. The EDS analysis of the obtained products (Figure 5(a)) indicates $NiTiO_3$ nanocrystals are composed of titanium, nickel, silicon, and oxygen with an approximate molar ratio of Ni/Ti $\approx$ 1/1, which gives stoichiometric formula of as-obtained product $NiTiO_3$ with no chemical segregation phenomenon. The Si peak in the spectrum is from the silicon chip for making sample. It can be seen from Figure 5(b) that $NiTiO_3/TiO_2$ nanocomposites are composed of plentiful Ti, which can be explained by $TiO_2$ particles forming and covering at the surface of $NiTiO_3$ nanoparticles.

*3.4. Chromatic Properties and Diffuse Reflectance of Samples.* With the temperature increasing, the band gap decreases from 2.63 to 2.03 eV, which can be attributed to the decrease of O-M distance. The color of the pigment samples changes from yellow-green color to dark yellow and then to light yellow (Figure 6).

Table 2: Color coordinates of $NiTiO_3$ pigment samples.

| Calcining temperature | Color coordinates | | | |
|---|---|---|---|---|
| | $L^*$ | $\alpha^*$ | $b^*$ | $c^*$ |
| $NiTiO_3$ | | | | |
| 700°C | 73.0 | −6.2 | 10.2 | 11.9 |
| 750°C | 67.4 | −3.99 | 42.1 | 42.3 |
| 800°C | 61.0 | 4.56 | 49.8 | 50.0 |
| 850°C | 57.2 | 5.14 | 48.7 | 48.9 |
| 900°C | 54.4 | 6.59 | 48.0 | 48.5 |
| $NiTiO_3/TiO_2$ | 62.4 | 3.21 | 32.5 | 32.7 |

The chromatic properties of the obtained $NiTiO_3$ pigment samples can be assessed from their CIE 1976 $L^*\alpha^*b^*$ color coordinate values, which are listed in Table 2. It can be seen for $NiTiO_3$ that, with the temperature increasing, the decreasing of $L^*$ value (from 73.0 to 54.4) indicates the enhancing of the darkness of pigments. $L^*$ value of $NiTiO_3/TiO_2$ nanocomposites is lower than that of pure $NiTiO_3$ obtained at 700°C. $a^*$ value regularly changes from −6.20 to 6.59, which indicates weakening of the green hue of the pigments. From

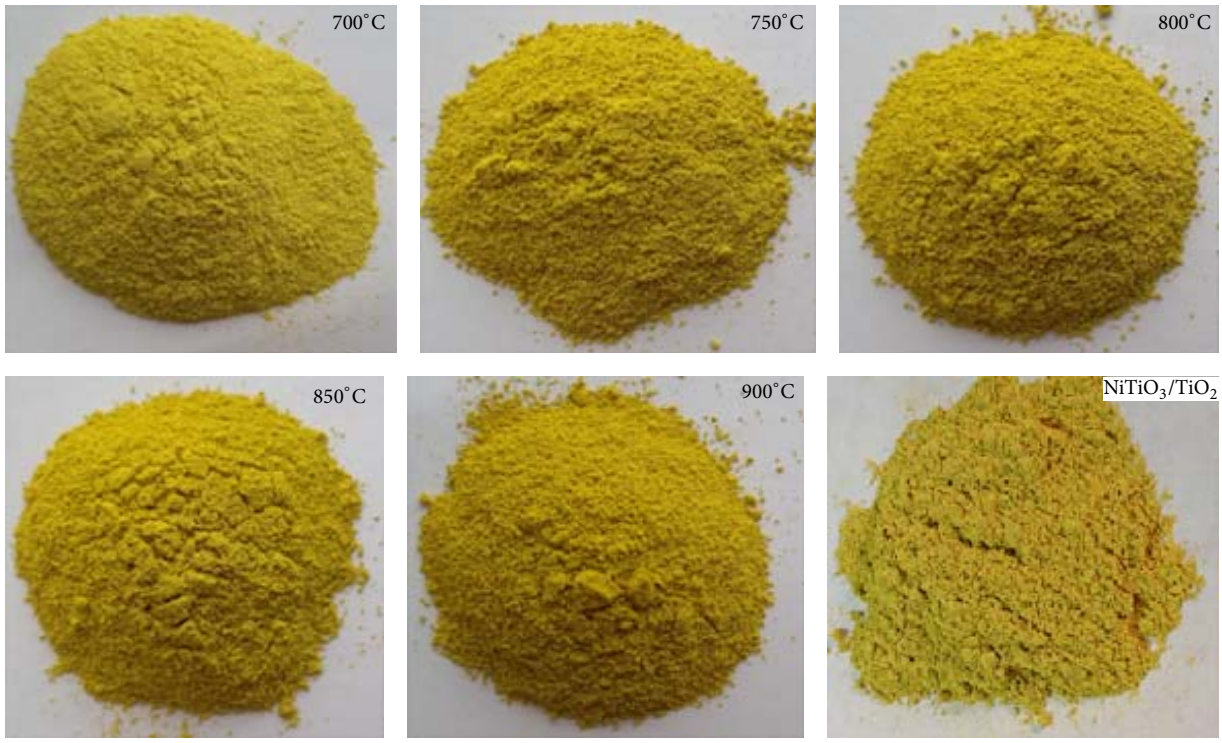


Figure 6: Photographs of $NiTiO_3$ pigments calcined at 700°C, 750°C, 800°C, 850°C, and 900°C for 4 h and $NiTiO_3/TiO_2$ composites.

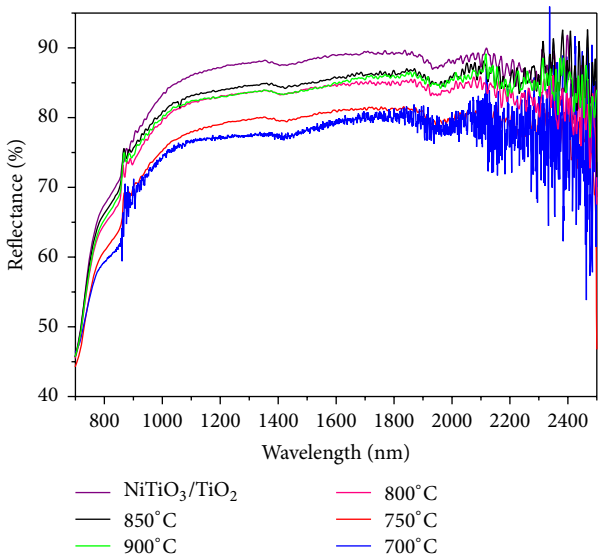


Figure 7: NIR reflectance spectra of $NiTiO_3$ nanopigments and $NiTiO_3/TiO_2$ composites.

$b^*$ value, it can be noted that the yellowness of pigments achieves maximum at calcining temperature of 800°C. The values are reasonable and consistent with the results from Figure 6.

The NIR reflectance spectra of the $NiTiO_3$ nanocrystals obtained at different temperatures are given in Figure 7. The $NiTiO_3/TiO_2$ composite sample processes higher NIR reflectance of about 89.7% compared with pure $NiTiO_3$ sample of 87.5%. By composite $NiTiO_3$ and $TiO_2$, the pigments have yellow color and higher NIR reflectance. From this, it can be seen that there exists the synergetic effect between $NiTiO_3$ and $TiO_2$. Therefore, the high NIR reflectance (~89.7%) showed by the yellow composite colored pigments will make them interesting candidates for use as cool colorants.

## 4. Conclusions

Highly dispersed $NiTiO_3$ nanocrystals and $NiTiO_3/TiO_2$ composite pigments have been synthesized. All the peaks in XRD patterns were indexed. SEM micrographs revealed that $NiTiO_3$ sample had good dispersibility and uniform size distribution. The morphologies of $NiTiO_3/TiO_2$ nanocomposites are shown as uniform and highly dispersed $NiTiO_3/TiO_2$ nanoparticles with spherical shape. The optical data of $NiTiO_3$ sample were analyzed at the near-absorption edge. With the temperature increasing, the band gap decreases from 2.63 to 2.03 eV, which can be attributed to the decrease of O-M distance. The color of the pigment samples changes from yellow-green color to dark yellow and then to light yellow. The $NiTiO_3/TiO_2$ composite sample processes higher NIR reflectance of about 89.7%. Moreover, the obtained pigments do not encompass any toxic metal element and can be considered as interesting candidates for use in the surface coating application as cool colorants.

## Competing Interests

The authors declare that there are no competing interests regarding the publication of this paper.

## Acknowledgments

The authors gratefully acknowledge the financial support of Key Programs for Science and Technology Development of Henan province, China (no. 122102210239), the Fund for Young Teachers in University of Henan Province, China (2012GGJS-103), the key science and technology plan projects of Zhengzhou city (no. 131PPTGG410-12), and the Natural Science Research Projects of Education Department of Henan province, China (13B560115).

## References

[1] P. Jeevanandam, R. S. Mulukutla, M. Phillips, S. Chaudhuri, L. E. Erickson, and K. J. Klabunde, "Near infrared reflectance properties of metal oxide nanoparticles," *Journal of Physical Chemistry C*, vol. 111, no. 5, pp. 1912–1918, 2007.

[2] S. Jose and M. L. Reddy, "Lanthanum-strontium copper silicates as intense blue inorganic pigments with high near-infrared reflectance," *Dyes and Pigments*, vol. 98, no. 3, pp. 540–546, 2013.

[3] G. George, V. S. Vishnu, and M. L. P. Reddy, "The synthesis, characterization and optical properties of silicon and praseodymium doped Y6MoO12 compounds: environmentally benign inorganic pigments with high NIR reflectance," *Dyes and Pigments*, vol. 88, no. 1, pp. 109–115, 2011.

[4] A. K. V. Raj, P. Prabhakar Rao, S. Sameera, and S. Divya, "Pigments based on terbium-doped yttrium cerate with high NIR reflectance for cool roof and surface coating applications," *Dyes and Pigments*, vol. 122, pp. 116–125, 2015.

[5] T. Thongkanluang, P. Limsuwan, and P. Rakkwamsuk, "Preparation and application of high near-infrared reflective green pigment for ceramic tile roofs," *International Journal of Applied Ceramic Technology*, vol. 8, no. 6, pp. 1451–1458, 2011.

[6] M. C. Zhao, A. J. Han, M. Q. Ye, and T. T. Wu, "Preparation and characterization of $Fe^{3+}$ doped $Y_2Ce_2O_7$ pigments with high near-infrared reflectance," *Solar Energy*, vol. 97, pp. 350–355, 2013.

[7] J.-L. Wang, Y.-Q. Li, Y.-J. Byon, S.-G. Mei, and G.-L. Zhang, "Synthesis and characterization of $NiTiO_3$ yellow nano pigment with high solar radiation reflection efficiency," *Powder Technology*, vol. 235, pp. 303–306, 2013.

[8] S. Moghiminia, H. Farsi, and H. Raissi, "Comparative optical and electrochemical studies of nanostructured $NiTiO_3$ and $NiTiO_3$-$TiO_2$ prepared by a low temperature modified Sol-Gel route," *Electrochimica Acta*, vol. 132, pp. 512–523, 2014.

[9] G. R. Yang, W. Chang, and W. Yan, "Fabrication and characterization of $NiTiO_3$ nanofibers by sol-gel assisted electrospinning," *Journal of Sol-Gel Science and Technology*, vol. 69, no. 3, pp. 473–479, 2014.

[10] J. B. Bellam, M. A. Ruiz-Preciado, M. Edely, J. Szada, A. Jouanneaux, and A. H. Kassiba, "Visible-light photocatalytic activity of nitrogen-doped $NiTiO_3$ thin films prepared by a co-sputtering process," *RSC Advances*, vol. 5, no. 14, pp. 10551–10559, 2015.

[11] M. A. E. Gabal, Y. M. A. Angari, and A. Y. Obaid, "Structural characterization and activation energy of $NiTiO_3$ nanopowders prepared by the co-precipitation and impregnation with calcinations," *Comptes Rendus Chimie*, vol. 16, no. 8, pp. 704–711, 2013.

[12] M. S. Sadjadi, K. Zare, S. Khanahmadzadeh, and M. Enhessari, "Structual characterization of $NiTiO_3$ nanopowders prepared by stearic acid gel method," *Materials Letters*, vol. 62, no. 11, pp. 3679–3681, 2008.

[13] Y. P. Tong, S. B. Zhao, L. Ma, W. X. Zhao, W. H. Song, and H. Yang, "Facile synthesis and crystal growth dynamics study of $MgAl_2O_4$ nanocrystals," *Materials Research Bulletin*, vol. 48, no. 11, pp. 4834–4838, 2013.

[14] Y. P. Tong, S. B. Zhao, X. Wang, and L. D. Lu, "Synthesis and characterization of $Er_2Sn_2O_7$ nanocrystals by salt-assistant combustion method," *Journal of Alloys and Compounds*, vol. 479, no. 1-2, pp. 746–749, 2009.

[15] Y. Qu, W. Zhou, L. Jiang, and H. Fu, "Novel heterogeneous CdS nanoparticles/$NiTiO_3$ nanorods with enhanced visible-light-driven photocatalytic activity," *RSC Advances*, vol. 3, no. 40, pp. 18305–18310, 2013.